Mechanistic Basis of Conductivity in Carbon Dioxide-Expanded Electrolytes: A Joint Experimental-Theoretical Study

Christian K. Nilles,[a,b] Ashley K. Borkowski,[b] Elizabeth R. Bartlett,[b] Matthew A. Stalcup,[a,c,#] Hyun-Jin Lee,[a] Kevin C. Leonard,*[a,c] Bala Subramaniam,*[a,c] Ward H. Thompson,*[a,b] and James D. Blakemore*[a,b]

[a] Center for Environmentally Beneficial Catalysis, University of Kansas, 1501 Wakarusa Drive, Lawrence, Kansas 66047, United States

[b] Department of Chemistry, University of Kansas, 1567 Irving Hill Road, Lawrence, Kansas 66045, United States

[c] Department of Chemical and Petroleum Engineering, University of Kansas, 1530 W 15th Street, Lawrence, Kansas 66045, United States

[#] Current address: Sandia National Laboratory, Eubank Blvd SE, Albuquerque, New Mexico 87123, United States

KEYWORDS: Pressure; Electrochemistry; Molecular Simulations; Diffusion; Ion Pairing

ABSTRACT: Electrolyte conductivity contributes to the efficiency of devices for electrochemical conversion of carbon dioxide (CO_2) into useful chemicals, but the effect of dissolution of CO_2 gas on conductivity has received little attention. Here, we report a joint experimental-theoretical study of the properties of acetonitrile-based CO_2-expanded electrolytes (CXEs) that contain high concentrations of CO_2 (up to 12 M), achieved by CO_2 pressurization. Cyclic voltammetry data and paired simulations show that high concentrations of dissolved CO_2 do not impede the kinetics of outer-sphere electron transfer but decrease solution conductivity at higher pressures. In contrast with conventional behaviors, Jones reactor-based measurements of conductivity show a non-monotonic dependence on CO_2 pressure: a plateau region of constant conductivity up to ca. 4 M CO_2 and a region showing reduced conductivity at higher $[CO_2]$. Molecular dynamics simulations reveal that while the intrinsic ionic strength decreases as $[CO_2]$ increases, there is a concomitant increase in ionic mobility upon CO_2 addition that contributes to stable solution conductivities up to 4 M CO_2. Taken together, these results shed light on the mechanisms underpinning electrolyte conductivity in the presence of CO_2 and reveal that dissolution of CO_2, although nonpolar by nature, can be leveraged to improve mass transport rates, a result of fundamental and practical significance that could impact the design of next-generation systems for CO_2 conversion. Additionally, these results show that conditions where ample CO_2 is available at the electrode surface are achievable without sacrificing the conductivity needed to reach high electrocatalytic currents.

1. INTRODUCTION

Molecular-level electrolyte design holds great promise as a strategy for improving the selectivity, efficiency, and stability of electrochemical processes.[1,2,3] This is because of the recognized importance of fundamental, intermolecular interactions in governing the structure of the electrochemical double layer and the reaction-diffusion region near electrodes in which electrochemical and electrocatalytic processes take place.[4,5] Modifications to the structure and composition of these critical microenvironments have been demonstrated to result in dramatic changes in chemical reaction outcomes, particularly in the arena of electrosynthetic work.[6]

Within the booming field of electrochemical carbon dioxide (CO_2) conversion and utilization, numerous studies have explored how microenvironment tuning affects catalysis.[7,8,9,10] An important example of such behavior is the addition of Lewis acidic cations to aqueous electrolytes; cations have been shown to impart changes in local electric fields and solvation effects, resulting in enhanced product yields.[11,12,13] Similarly, very impactful work has demonstrated how the composition and structure of layered gas-diffusion electrodes (GDEs) can be used to significantly improve selectivity for the generation of multi-carbon products from CO_2 in electrolyzers.[14,15] In these electrolyzers, the GDEs appear to enable improved local concentrations of available CO_2 for conversion.[16]

In our recent work, we have been developing CO_2-rich organic electrolyte solutions as media for electrocatalytic CO_2 conversion, motivated by the apparent requirement in electrocatalysis for high substrate concentrations near the electrode surface to enable robust turnover.[17,18] In our media, multi-molar concentrations of CO_2 can be achieved at pressures (10-800 psi) that are milder than those needed to generate supercritical CO_2 (1071 psi).[19,20] Because the volume of the liquid phase expands with increasing CO_2 pressure — to the extent that it is visible to the naked eye in an appropriate view cell — we have termed these media as CO_2-eXpanded Electrolytes (CXEs). We have experimentally confirmed a nearly exponential increase in dissolved CO_2 in CXEs up to 15 M or so, as shown in Figure 1, opening a wide chemical space of CO_2 concentrations for exploration, which contrasts with a rather limited concentration space afforded by near-ambient work in the field.

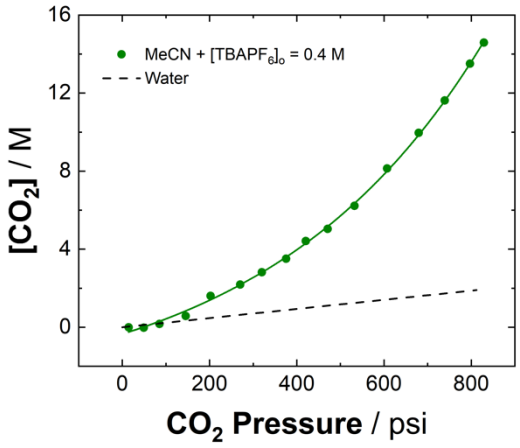

Figure 1. Pressure-dependent concentration of CO_2 in CXEs. The dotted black line is the concentration of CO_2 in water based on Henry's law calculations.

Considering the significant activity across disciplines around electrolyte engineering and CO_2 conversion,[21] it is surprising that few studies have examined the consequences of dissolution of high millimolar to molar quantities of CO_2 in media used for electrochemistry.[22] In part, this lack of attention may be attributable to the multiple, interrelated phenomena involved: dissolution of CO_2 into liquids has been shown to result in decreased overall polarity (dielectric constant),[23] increased diffusivity of solution components,[24] decreased charge screening, and increased ion pairing in cases where ions are present.[25] However, to the best of our knowledge, these molecular phenomena have not been explored in the context of CO_2-rich electrolyte engineering. In light of the opportunities afforded by CXE media, we anticipated that quantification of the effect of CO_2 dissolution on solution conductivity in CXEs could afford an experimental platform upon which to explore the fundamental interactions impacted by dissolution of large concentrations of CO_2. We also anticipated that joint theoretical work could examine the dielectric, diffusive, and electrostatic contributions to electrolyte behavior, informing the use or design of electrolytes for specific applications.

Here, we report a joint experimental-theoretical investigation of the molecular behaviors and fundamental interactions that underpin the CO_2-concentration-dependent solution conductivity of organic electrolytes containing acetonitrile (MeCN) and tetrabutylammonium hexafluorophosphate ($TBAPF_6$). Contrasting with conventional liquid-phase behavior wherein dilution of the ionic charge carriers of the electrolyte results in a linear decrease in solution conductivity, molecular dynamics (MD) simulations reported here show that at moderate concentrations, the high diffusivity of CO_2 effectively serves to diminish the consequences of its low dielectric constant. Solution conductivity data in conventional electrolytes and CXEs were measured in a reactor cell appropriate for pressure-dependent electrochemistry with a custom-fabricated Jones-geometry apparatus that was based on analogous devices reported for use at ambient pressures; simulations of cyclic voltammetry data from three-electrode measurements also support the conclusions drawn from the theoretical work. Taken together, our findings provide a comprehensive picture of the molecular influences that CO_2 can exert on organic electrolyte solutions.

2. RESULTS

2.1. Quantification of CO_2 Dissolution at Pressure with Volumetric Expansion. Our CXEs are conceptually related to an established class of organic media known as CO_2-eXpanded Liquids (CXLs) and can be well understood in this context, particularly from the standpoint of their vapor-liquid equilibrium (VLE) behavior.[26,27,28] Summarizing, at the relatively mild pressures explored in this work, the critical properties of CO_2 ($T_{critical}$ = 31.1 °C; $P_{critical}$ = 1071 psi) drive a nearly exponential increase in liquid-phase gas solubility in organic solvents such as acetonitrile. The pressure range explored in our studies here (up to ca. 800) psi) can be judged as mild relative to pressures utilized in certain industrial processes that are currently practiced on large scales (see Discussion Section for more details). Although work under pressure imposes an energy penalty in any case, significant advantages can be exploited, as we describe in this work. The increased solubility of CO_2 under pressurization is one of these key advantages. The improved solubility leads to significant volumetric expansion (VE) of the liquid phase; the VE must be quantified for work in expanded media to proceed, as the pressure dependence of the liquid phase volume must be determined. With knowledge of this relationship in hand, the concentration of analytes of interest that are present can be reliably determined for chemical work. The VE properties of pure MeCN pressurized with CO_2 have been known for many years,[28] but as electrochemical experiments require electrolytes, our prior work[19] expanded the knowledge of VE to electrolyte-containing MeCN-based solutions for the first time.

In the work reported here, the concentration of the electrolyte salt was fixed at a given concentration prior to pressurization with CO_2, in order to enable controlled conditions and comparison of measurements made upon pressurization. Measurements of the VE properties of specific electrolyte solutions upon pressurization were required to obtain the pressure-dependent concentrations of the MeCN and supporting electrolyte salt, and offered the prospect of examining the influence of electrolyte concentration on the volumetric expansion behavior itself. Consequently, our work here began with measurement of the pressure-dependent properties of acetonitrile solutions containing the $TBAPF_6$ electrolyte. $TBAPF_6$ was selected for this work as it is among the workhorse electrolytes used for organic electrochemistry and it is commercially available. As shown in Figure 2, the addition of 0.4 M $TBAPF_6$ to pure, dry MeCN does not impede the formation of expanded media that contain high CO_2 concentrations (Figure 2, green points). The addition of supporting electrolyte to MeCN, however, does result in a flattening of the curve for subsequent volumetric expansion of that solution, meaning that less gas can be dissolved. However, the solution in all cases here remains capable of holding significant amounts of CO_2, comparing well with neat MeCN. Increasing the $TBAPF_6$ concentration to 1.0 M (Figure 2, orange points) further depresses the volumetric expansion, a behavior in line with the other two cases shown here which suggests that expansion of the MeCN component of the solution is responsible for the ability to form CXE media. And, we note here that in both the cases of addition of either 0.4 M or 1.0 M $TBAPF_6$ to the starting MeCN solution, expansion with CO_2 does not cause precipitation of the electrolyte.

For comparison to these findings, use of water as a solvent leads to minimal volumetric expansion, as shown in the relevant literature.[26] Similarly, the concentration of CO_2 in H_2O as a function of pressure is constrained by Henry's Law (see Figure 1), resulting in an essentially linear increase in the concentration of CO_2 in H_2O; this linear behavior contrasts markedly with the more significant, virtually exponential increase in CO_2 concentration that can be achieved by using MeCN as the cosolvent for gas dissolution.

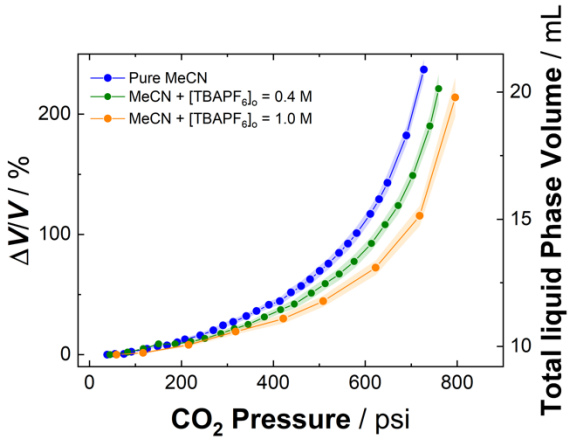

Figure 2. VLE curves at 25°C with CO_2 pressurization at varying initial amounts of $TBAPF_6$. Uncertainty associated with the VLE data is given as ±1σ, and was determined from triplicate data sets.

2.2. Electrochemical Simulations. The VE data shown in Figure 2 represent a continuum of pressure-tunable media containing large amounts of CO_2. The amount of CO_2 present at a given pressure was quantified in our prior measurements that extracted the CO_2 concentration for the case where $[TBAPF_6]_0 = 0.4$ M.[19] Here, our goal is to directly interrogate the effects of the dissolved CO_2 on the electrochemical properties of the resulting CXEs at our accessible range of pressures. Initially, we focused our work on the electrochemical response of ferrocene under CXE conditions; we selected ferrocene as our redox-active probe molecule in light of this species' solubility in CXE media as well as its (electro)chemical stability.[29] Ferrocene has also been established to display intrinsically fast electron transfer behavior, making it attractive for judging the ideality of voltammetry under various conditions.[30] In the past, we have found ferrocene is soluble in CXEs and that its Fe(III)/Fe(II) reduction potential in CXEs remains similar to the established value under routine conditions in MeCN-based electrolytes.[19]

Pressurization of solutions containing an initial concentration of 0.4 M $TBAPF_6$ in a Parr reactor outfitted with a custom-designed cap with appropriate feedthroughs for electrochemical studies revealed that the iron-centered redox cycling of dissolved ferrocene could be measured by cyclic voltammetry (CV) over the full range of CO_2 pressures accessible in our CXE media (see Figures 3 and S2). The ferrocene redox couple measured under these conditions retained the conventional, quasi-reversible appearance of this fast redox couple, in line with the expected chemical stability of both the Fe(II) and Fe(III) forms of the compound in CXEs. However, the peak-to-peak separation (ΔE_p) displayed by this redox couple grows systematically larger as the applied CO_2 pressure is increased (Figure 3 and Figure S2). On the one hand, the CO_2 pressure dictates the concentration of CO_2 present in the CXE media; thus, the dissolution of CO_2 can be identified as being causative for this change in ΔE_p. On the other hand, there are two primary mechanistic origins that could be responsible for the increased ΔE_p: an increased resistance of the bulk solution or a decrease in the heterogeneous electron transfer kinetics for ferrocenium/ferrocene redox cycling.[31]

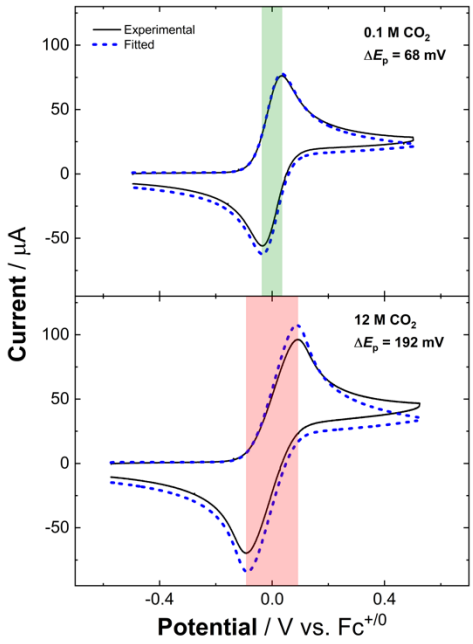

Figure 3. Experimental and simulated cyclic voltammetry of $Fc^{+/0}$ collected at 50 (0.1 M CO_2) and 740 psi CO_2 (12 M CO_2). Shaded areas are Fc peak-to-peak separation. Conditions: working electrode HOPG, counter electrode Pt wire, reference electrode Pt wire, and scan rate 100mV/s.

To distinguish these possible origins for the increased peak-to-peak separation, we turned to simulation and fitting of our electrochemical data using the DigiElch software package. We were focused on investigating pressure-dependent changes in solution resistance (R_{Sol}) and/or heterogeneous electron transfer rate ($k°$), so we input the $1e^-$ process for chemically reversible oxidation/reduction of ferrocene/ferrocenium as the electrode-driven process to be modeled by the program. Our experimental voltammograms were also loaded into the software for fitting and extraction of key variables, but we do note that relevant experimentally known values for certain quantities were also input to the software, including the double-layer capacitance (1.0×10^{-5} F),[32] area of our working electrode (0.15 cm^2), temperature (25°C), and pressure-corrected concentration of ferrocene in solution (2 mM). On the basis of the appearance of the voltammetry and the well-established molecular properties of ferrocene, we set the initial value of the charge transfer coefficient (α) to 0.5. The potential for the single iron-centered redox couple in our data was also input, and was fixed for purposes of the simulations, in line with the previously measured pressure-independence of the potential. In terms of the fitting process, we explored both allowing the determining parameters (R_{Sol}, $k°$) to float as well as manually simulating individual sets of values for these variables to explore trends.

Satisfactory agreement between the experimental and simulated data could only be obtained when the value of the solution resistance (R_{Sol}) in the model was increased as a function of increasing pressure. At near-ambient conditions, the solution resistance was ca. 60 Ω, but the estimated resistance markedly increased up to ca. 470 Ω at 740 psi (see Table 1). On the other hand, satisfactory fits to the voltammetry could not be obtained when the corresponding heterogeneous electron transfer rate ($k°$) was varied from fast to slow across the pressure range studied. Notably, a sensitivity study of the effect of decreasing the value of $k°$ in the model revealed that, although ΔE_p was dependent on $k°$ as expected and increased as the electron transfer rate was decreased, the overall agreement between the experimental and simulated voltammetry profiles was poor when manipulating these two variables simultaneously. The overall shapes of simulated waves for ferrocenium/ferrocene

Table 1. Pressure tunability of electrochemical properties of $[0.4\ M\ TBAPF_6]_0$ MeCN solution containing ferrocene.

Pressure / psi	**50**	**250**	**450**	**550**	**650**	**740**
$[CO_2]$ / M	0.1	1.8	4.8	6.9	9.3	11.7
$[TBAPF_6]$ / M	0.40	0.36	0.30	0.26	0.21	0.15
$\Delta E_{P(Ex)}$ / mV	68	77	92	85	100	192
$\Delta E_{P(Sim)}$ / mV	69	69	77	82	95	175
D_o / x10^{-5} cm^2 s^{-1} [a]	0.9	0.9	1.4	1.4	1.5	3.1
D_R / x10^{-5} cm^2 s^{-1} [a]	0.9	0.9	1.6	1.6	1.2	2.0
R_{Sol} / Ω [b]	57 ± 1	58 ± 1	75 ± 1	91 ± 1	167 ± 1	470 ± 1

[a]Diffusion coefficients were determined through simulations of experimentally collected $Fc^{+/0}$ cyclic voltammetry at each pressure. [b]Resistance values collected through EIS measurements. Uncertainty (given as ±1σ) was calculated from EIS measurements at 1,0, −1 V vs. $Fc^{+/0}$.

redox were poor matches to the experimental data when only $k°$ was modulated (see Figure S1). Experimental measurement of R_{Sol} using electrochemical impedance spectroscopy (EIS) returned values that could be used in the simulations to obtain reasonable agreement between the experimental and modeled voltammograms (see Table 1).

The diffusion coefficients for ferrocene (D_R) and ferrocenium (D_O) were also determined through these simulations, and the resulting values show that pressurization with CO_2 also drives an increase in these quantities, particularly at the highest pressures (see Table 1). These observations are consistent with our working hypothesis that CO_2 dissolution results in the liquid phase becoming more "gas-like" in its behavior and thus produces greater mobilities of species present under pressurized conditions. This trend is also consistent with observations of improved mass transport in CXL media.[33] The observation of enhanced diffusion of ferrocene and ferrocenium upon CO_2 pressurization is also consistent with the results of theoretical calculations carried out in the course of this work (*vide infra*).

2.3. Conductivity. Modeling of the cyclic voltammetry data revealed that the composition of our CXE media impacts most of the key features of the electrochemical response. We anticipated that a key driver of these changes was the pressure-dependence of the solution conductivity (σ), and thus pursued rigorous measurements of σ under our experimental, pressurized conditions. It was necessary to collect the conductivity data in a standardized, appropriate manner that would be ultimately compatible with theoretical simulations; therefore, we designed and constructed a Jones-geometry device to measure the conductivity of CXE media under pressure.[34] The solution conductivity, σ, represents the intrinsic ability for a solution containing cations and anions to carry current during electrochemical experiments. Our device was designed to withstand pressure while being in line with NIST recommendations for measurement of intrinsic conductivity values, thus facilitating comparisons across conditions (see Experimental Section for details). The conductivity, σ, of a solution is defined by Eq. 1 and calculated from the cell constant (the ratio of distance separating the parallel-facing working (l) and their cross-sectional areas (A), divided by the solution resistance measured by EIS:

$$\sigma = \frac{\left(\frac{l}{A}\right)}{R_{sol}} \qquad (1)$$

The conductivity data collected across the full pressure range for our CXE media are shown in the blue points in Figure 4, revealing two regimes of behavior. In the first regime, we observed a virtually pressure-independent behavior wherein the solution conductivity was found to be invariant as a function of CO_2 pressure. This invariance with pressure held despite the dilution of the dissolved electrolyte from the initial concentration of 0.4 M down to ca. 0.31 M. In the second regime, with pressures of CO_2 around 450 psi and greater, we measured a linear decrease in conductivity. Prior findings from the literature show that, under conventional conditions, solution conductivity decreases linearly with decreasing ionic strength.[35] Thus, our findings in these CXEs contradict this expected behavior, based only on ionic concentration. However, as previously stated, this is not the sole factor that contributes to conductivity, and thus other effects, identified by molecular dynamics simulations (*vide infra*), must also be taken into account.[36]

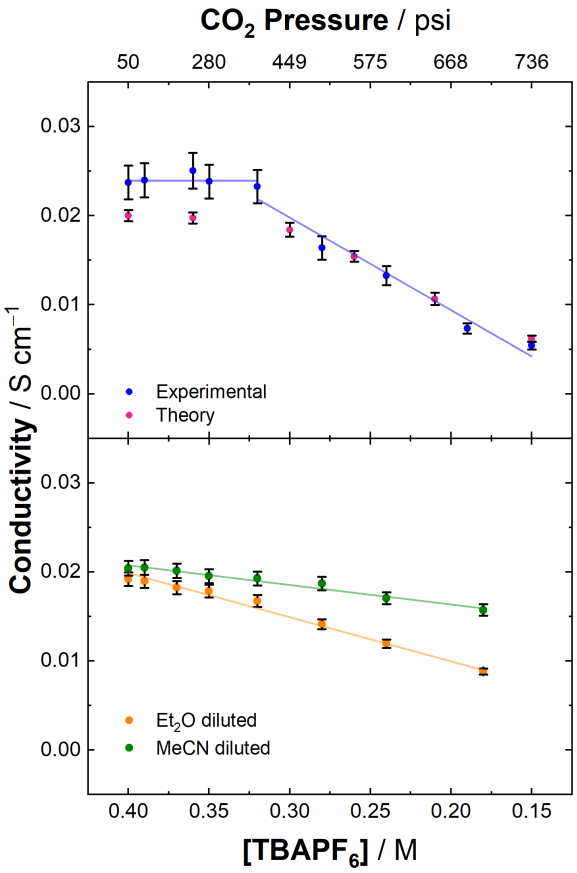

Figure 4. Experimental (0.4 M $TBAPF_6$ MeCN) and theoretical (0.4 M $TPrAPF_6$ MeCN) conductivity of the solution with increasing amounts of CO_2. Experimental uncertainty (top panel) is derived from replicate EIS measurements at ~500 psi CO_2 (Figure S6) and is shown at the 68% confidence interval (±1σ). Uncertainty in the theory values were calculated using block averaging over 5 simulations and shown at the 95% confidence interval using Student's t-distribution. Uncertainties for bottom panel are 68% confidence intervals (±1σ) were calculated from replicate EIS measurements of initial 0.4 M $TBAPF_6$ MeCN solution (Figure S5).

Having observed the unconventional case of two different regimes of pressure-dependent solution conductivity in the data shown in Figure 4, we next moved to collect complementary data that could identify any unique features obtained from dilution of our electrolyte solution with CO_2 rather than a more traditional diluent such as a second liquid organic solvent. For this purpose, we used two different liquid organic solvents, acetonitrile (MeCN) and diethyl ether (Et_2O). In both cases, an initial solution with $[TBAPF_6]_0$ = 0.4 M in MeCN was prepared, and conductivity measurements with our Jones-type device were collected as a function of dilution of the starting solution with either further MeCN or Et_2O. In the case of MeCN dilution, the measured conductivity decreases in a virtually linear fashion upon dilution of the $TBAPF_6$ concentration (Figure 4, green points). This also appears to be the case with Et_2O dilution; dilution of the electrolyte solution with Et_2O shows a nearly linear decrease in conductivity. However, there does appear to be a slight curvature to the decrease in the case of Et_2O, most apparent around 0.325 M (Figure 4, orange points). This slight deviation from linearity could be attributed to the differences in viscosity between MeCN and Et_2O; use of Et_2O can be safely concluded to decrease solution viscosity and enhance diffusion of the ions. (The viscosities of neat MeCN and Et_2O are 0.369 and 0.224 mPa•s, respectively.[37]) We emphasize however that the deviation from a single, linear behavior as displayed by conventional solutions is most significant in the case of dilution with CO_2 in Figure 4 blue points.[35]

In addition to the slight deviation from linearity in the dilution-dependent conductivity data using Et_2O, we also identified several other key insights. The more negative slope/dependence of the conductivity-vs-concentration plot obtained for the case of dilution with Et_2O can be superficially understood to arise due to the smaller dielectric constant of Et_2O (4.27) in comparison to that of MeCN (36.64).[37] In the case of Et_2O, the lower dielectric constant can be identified as driving decreased charge stabilization/screening, with the result of greater anion/cation pairing in solution as the overall polarity of the medium decreases. In the case of dilution with MeCN, there is a less significant change in polarity as the concentration of the electrolyte decreases, resulting in minimal increases in ion pairing in solution and thus a less significant drop in solution conductivity as the overall electrolyte concentration is decreased. This trend observed with the MeCN dilution was further confirmed with MD simulations with good agreement found between the experimental and theoretical data (Figure S7). Upon seeing these trends, we hypothesized that ion concentration alone is not the key determinant of the two-regime behavior observed in Figure 4, rather, we hypothesized that CO_2-induced modulations of anion-cation interactions and individual ion mobilities could contribute as well. Inspection of the slopes of the linear regions in the data shown in Figure 4 provides an indication that this may be the case, as the slope for dilution with CO_2 (-0.10 S cm^{-1} M^{-1}) is approximately twice as negative as that found in the case of Et_2O dilution (-0.05 S cm^{-1} M^{-1}). This situation can be ascribed to the nonpolar nature of CO_2.

As electrolytic conductivity is affected by the solution mobilities of the cations and anions present, we turned back to our CV data and modeling work (Sec. 2.2) to search for any indications of pressure-dependent changes in mobility. Indeed, we observed that the diffusion of both ferrocene and ferrocenium accelerate as $[CO_2]$ is increased in the liquid phase. This is evident in the generally increasing values of D_O and D_R at higher pressures (Table 1). However, we note here that the increased diffusivity of these redox-active molecules could be merely representative of greater overall diffusivities for all the molecules present in solution as the pressure is increased. Thus, the MeCN molecules as well as dissolved NBu_4^+ and PF_6^- ions should undergo faster diffusion as the CO_2 pressure is increased. Additionally, we note that the information from the voltammetry and related simulations, taken together with the rigorous measurements of conductivity in the Jones-geometry device, point to the same conclusion: the solution conductivities of CXE media are relatively constant at low-to-moderate pressures but decrease at higher pressures beyond a threshold value around 400 psi (cf. data in Table 1 and Figure 4). The qualitative conclusions are the same from both types of measurements, but the intrinsic solution conductivity is most appropriately quantified for comparisons in the Jones-geometry work. In order to decouple the individual influences of fundamental molecular interactions on the observed two-regime behavior of the pressure-dependent CXE conductivity measurements, we turned to MD simulations to rigorously quantify the various factors underpinning the observed regimes of experimental data.

2.4. Theory and Molecular Dynamics Simulations. The unconventional nature of the two-regime behavior in the experimental conductivity data shows, importantly, that even though the concentration of available electrolyte decreases up to CO_2 pressures of ca. 450 psi and beyond, the actual conductivity of the solution shows a virtually pressure-independent value. This indicates that, in an electrochemical system for CO_2 conversion at elevated pressures, there would be minimal additional resistive penalty up to an operating pressure of 450 psi. This provides a strong impetus for understanding the factors determining this behavior, which can provide key design principles for such electrocatalytic systems. To accomplish this we used MD simulations, which can

elucidate the molecular-level mechanistic details of how the ions interact with the solution components and how these interactions, in turn, influence the conductivity of the solution.

Molecular dynamics simulations were performed using the Large-Scale Atomic/Molecular Massively Parallel Simulator (LAMMPS).[38] Six systems were constructed to correspond with experimental ion concentrations within the range of experimental CO_2 pressures. In the MD simulations, the cation used was tetrapropylammonium ($TPrA^+$), a choice that simplifies the number of degrees-of-freedom for each individual cation while retaining the aliphatic-chain character of tetrabutylammonium, and the anion was hexafluorophosphate. The volume for each system was based on the initial electrolyte concentration (provided from experiment) and the fixed value of 20 ion pairs per system; the number of CO_2 molecules were then determined based on the measured CO_2 concentration for each pressure. Using the calculated equilibrium volume for each concentration, five constant volume and temperature simulations were propagated for a 1 ns equilibration, followed by a 25 ns production run at 298.15 K. Further simulation specifications and force-field parameters are included in the SI, see pp. S20-S23. From each 25 ns run, configurations and momenta were written every 50 fs. The mean squared-displacement (MSD), solution conductivity, shear viscosity, and radial distribution functions (RDFs) were calculated. Errors in the computed values were calculated using block averaging over the 5 simulations and were reported as 95% confidence intervals using the Student's *t*-distribution.[39]

Generalized diffusion coefficients were calculated from the MSDs, Eqs. 2-4 (see Experimental Section), for the ionic species in the system and are shown in Figure 5a. With increasing CO_2 pressure, the self-diffusion coefficients of both the cation and anions increase monotonically before plateauing around 550 psi. In addition to the cation and anion self-diffusion coefficients, the correlated displacements of the ions (cation-cation, anion-anion, and cation-anion) contribute to the solution conductivity via non-Nernst-Einstein effects[40] as indicated in Eqs. 5 and 6 (see Experimental Section). These terms quantify the correlation between the diffusive motion of different ions. They are also shown in Figure 5a and increase in magnitude with CO_2 pressure.

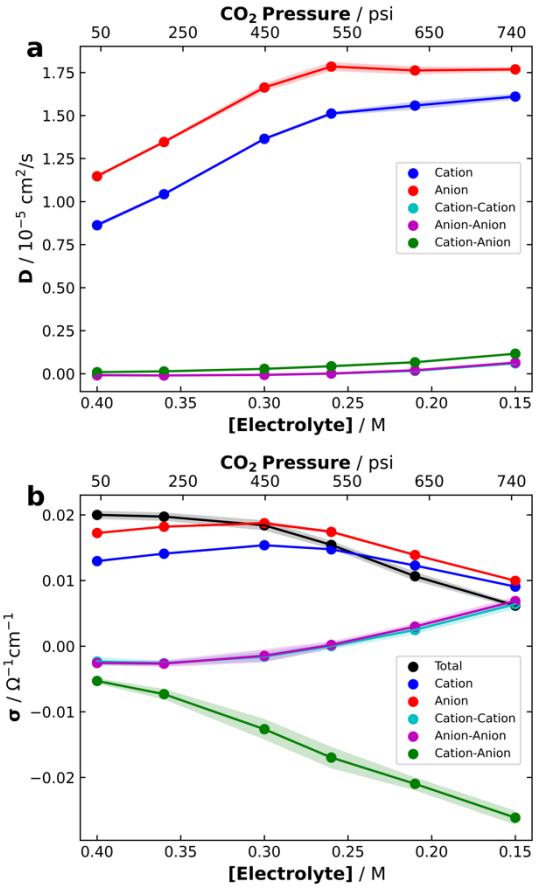

Figure 5. Ionic contributions to the (a) diffusion coefficients and (b) solution conductivity as a function of decreasing electrolyte concentration (increasing CO_2 pressure) are provided for the total (black), cation (blue), anion (red), cation-cation (cyan), anion-anion (magenta), and cation-anion (green) contributions. The data (in cyan) for cation-cation contributions are nearly identical to those for anion-anion contributions (in magenta).

Unlike the diffusion coefficients, the solution conductivity includes each factor weighted by the number of ions or ion pairs and divided by the volume (Eqs. 5 and 6; see Experimental Section). The simulated total conductivity shown in Figure 4 is also plotted in Figure 5b along with the different components just discussed. This correlated behavior of the ions, particularly at higher CO_2 pressure, shows that the Nernst-Einstein equation, which approximates the conductivity based only on the ion self-diffusion coefficients, is not a good approximation for the solution conductivity of this system. Therefore, we used the Einstein formula[41] to calculate the solution conductivity, as it incorporates these ionic correlated diffusion terms (Eqs. 5-7; see Experimental Section).

Using these methods, we obtained excellent agreement between our theoretically-predicted values of the pressure-dependent conductivity and the experimentally measured values (see Figure 4, pink and blue points, respectively). We see that the overall behavior of the solution conductivity is driven by the competing contributions from ion self-mobility and ionic correlated mobility (Figure 5b). At low CO_2 pressure, the solution conductivity is mainly represented by the contributions from the anion and cation self-diffusion, with minor inhibition from the cation-cation, anion-anion, and cation-anion correlated diffusion. Note that the solution conductivity includes a factor of the inverse solution volume, which leads to a decrease in the ion self-diffusion component with increasing expansion (ion dilution). In addition, as CO_2 pressure increases, the like-charge ionic correlated diffusion factors grow in,

showing the impact of repulsive forces to promote overall solution conductivity. At the same time, the opposite charge ionic correlated diffusion continues to decrease, becoming the competing factor of ionic attraction that ultimately drives the overall solution conductivity to decrease with increasing CO_2 pressure.

To elucidate the solution effects that contribute to these diffusion and solution conductivity behaviors, we investigated the viscosity of the solutions with varying electrolyte and CO_2 concentrations. The shear viscosity was calculated using the Green-Kubo relation (Eq. 8; see Experimental Section) by considering the time-correlated behavior of the pressure tensor autocorrelation function. We observe that as CO_2 pressure increases, the viscosity of the system dramatically decreases (Figure 6a). This can be directly correlated with the increased mobility of the ionic species in solution, and can be considered as a factor promoting solution conductivity. We also calculated the coordination number from the cation-anion radial distribution function (RDF) for each system (Eqs. 9 and 10; see Experimental Section) (Figure 6b). As CO_2 pressure increases, the average number of anion-cation ion pairs increases. At high CO_2 pressure, the system is greatly diluted, yet the anion-cation interactions increase. We can consider this as an effect of the decreased solution screening between ions due to increased incorporation of CO_2, a small, non-polar molecule. This behavior competes with the effects of the decreasing viscosity over the same regime, and further contributes to the concept that ion-pairing with simultaneous electrolyte dilution is the main driver of diminished solution conductivity at high pressures of CO_2.

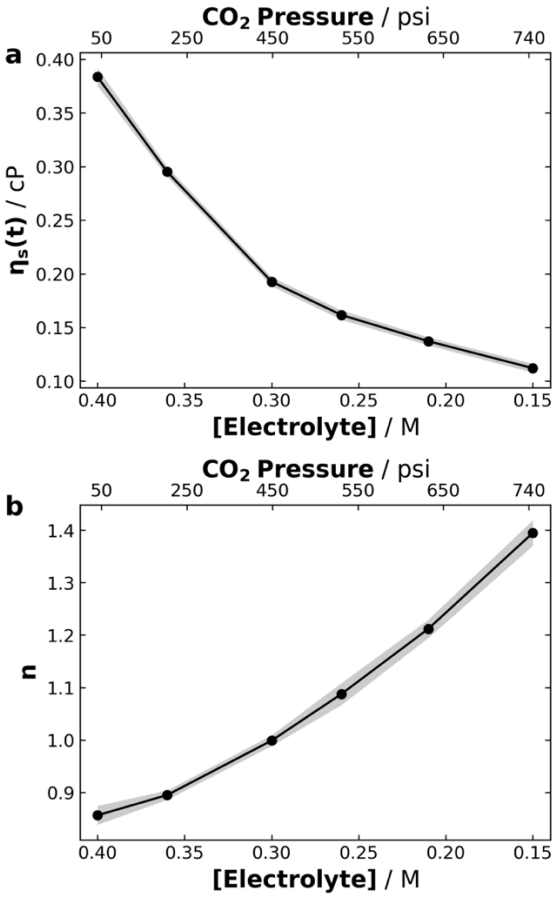

Figure 6. (a) Shear viscosity and (b) coordination number from the cation-anion RDF as a function of decreasing electrolyte concentration. Shaded regions show 95% confidence intervals.

2.5. Influencing Pressure-dependent Conductivity. The results of the MD simulations show that the pressure-dependent diffusivities of the anions and cations present in the electrolyte contribute to the solution conductivity, and that cross-interactions involving charge screening and ion pairing that are driven by the net solvent polarity can decrease conductivity. These observations suggest that both i) the pressure-independent regime of conductivity could be accessible at higher ionic strengths, and ii) that higher ionic strengths could drive even greater conductivities than those measured in our workhorse case of $[TBAPF_6]_0$ = 0.4 M.

Therefore, we explored the pressure-dependent conductivity of the higher ionic strength case where $[TBAPF_6]_0$ = 1.0 M. Using our VE data for this case (see Figure 2, orange points) and the Jones-geometry device, we measured conductivity over a similar range of pressures used for conductivity measurements at $[TBAPF_6]_0$ = 0.4 M (see Figure 7). On the one hand, the results show that increasing the concentration of supporting electrolyte ($[TBAPF_6]_0$ = 0.4 M vs. 1.0 M) results in an increase in conductivity; for example, at 700 psi, the conductivity increases from 0.0073 to 0.025 S cm^{-1}, respectively. This suggests that dissolution of additional ions into solution can overcome the ion pairing effect that is driven by dissolution of nonpolar CO_2 at higher pressures. On the other hand, the increase in conductivity is far less than the factor of 2.5 expected based only on concentration, especially at the highest CO_2 pressures. This is in accord with a greater tendency toward ion pairing at higher ionic strengths, particularly in the presence of high levels of dissolved CO_2. This observation shows that there is a diminishing return in terms of achieved conductivity when more electrolyte is dissolved, although gratifyingly, the regime of pressure-independent conductivity remains even at the conditions where $[TBAPF_6]_0$ = 1.0 M; this suggests that high-pressure organic electrochemical work with CO_2 is quite promising, in that conditions where ample CO_2 is available at the electrode surface are achievable without sacrificing the solution conductivity needed for establishing high currents in electrocatalysis.

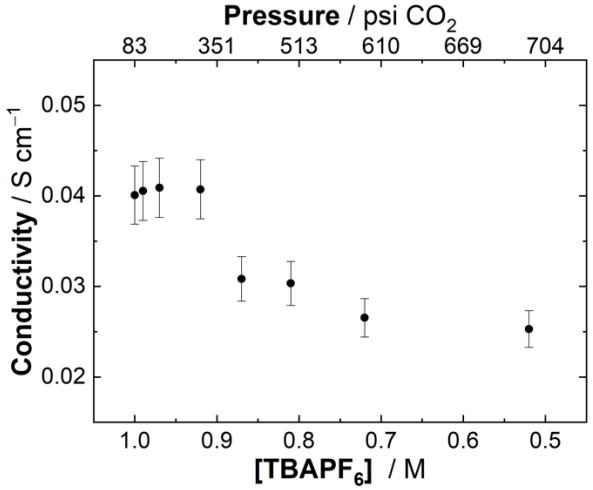

Figure 7. Conductivity of $[1.0\ M\ TBAPF_6]_0$ MeCN solution. Uncertainties (given as $\pm 1\sigma$) were calculated from replicate EIS measurements.

3. DISCUSSION

The electrolyte can be an overlooked component in electrochemical work, in that "off-the-shelf" electrolytes are often utilized without consideration of how results could be optimized by selection of a specific, tailored electrolyte or how the use of tunable conditions might affect results. However, the composition of the electrolyte has been shown to exert significant influences over electrochemical processes, as shown in a variety of both older and more recent works.[42,43,44] The two-regime

behavior revealed in the pressure-dependent conductivity data reported here fits into this theme, showing that dissolution of large (up to ~15 M) concentrations of CO_2 contributes to an unconventional conductivity profile. Theoretical work was used here to reveal the individual contributions of the fundamental behaviors of the ions in solution to these observations; the simple concentration of the electrolyte salt present in solution has been shown by this work not to be the sole factor that determines conductivity. This is unique, it appears, for the case where CO_2 is added to organic electrolytes at significant concentrations and contrasts with conventional/historical relationships that are understood to underpin ionic conductivity in organic solutions.[45]

We were motivated to pursue this study by the enduring interest in the chemistry and engineering communities toward using electrochemical and electrosynthetic methods to activate CO_2 for generation of more useful chemicals, either in direct electrocatalysis or perhaps electrosynthetic approaches pairing CO_2 with redox-active co-reactants. In both cases, we note that as CO_2 is a reactant; obtaining high space-time yields of products requires sufficiently high concentrations of CO_2 to support the current densities desired in the ultimate electrochemical devices.[46,47] Our work shows that high CO_2 concentrations can be achieved in CXEs without a major penalty in solution conductivity, and that dissolution of CO_2, although it is non-polar, can actually contribute helpfully to stable conductivity at low-to-moderate pressures. At the highest pressures, there is a penalty in conductivity for dissolving very high concentrations of CO_2. However, increasing the initial concentration of $TBAPF_6$ from 0.4 M to 1.0 M in our configuration results in an attenuation of this penalty (judged by the slopes of the linear regions in the data shown in Figures 4 and 7; see Figure S8); the CO_2-driven conductivity change drops from -5.2×10^{-5} S cm^{-1} psi^{-1} for the 0.4 M case to -3.5×10^{-5} S cm^{-1} psi^{-1} for the 1.0 M case. The different magnitudes of these slopes, along with the two-regime behavior highlighted above, point to the importance of understanding fundamental interactions when engineering electrolytes that can support the chemistry of interest in a given solution/device.

Turning to the implications of these findings for use of CXEs for catalytic CO_2 conversion and electrosynthesis,[17,18,19] we have previously observed an intriguingly common optimum pressure for conducting catalysis that is near 400-450 psi in all cases. In particular, our studies of the heterogeneous catalysis of CO_2-to-CO conversion on Au and electrosynthesis of atrolactic acid on carbon revealed parabolic activity-vs-pressure curves, with the optimum for both being around ca. 400-450 psi CO_2 (see Figure 8). In both these cases, the total yield of the targeted product and Faradaic efficiency of the overall processes were diminished at higher pressures.[17,19] Molecular electrocatalysis of CO_2-to-CO conversion with $Re(bpy)(CO)_3Cl$ in CXEs followed a similar trend, revealing a drop off in the rate of catalysis beyond 400 psi CO_2.[18] In all three of these cases, the loss of catalytic effectiveness at the highest pressures contradicts the intuitive picture that catalysis should be favored by increasing the amount of available substrate. However, even though outer-sphere electron transfer kinetics associated with ferrocene redox in the present work remained fast with increasing CO_2 pressure, in the two noted works regarding CO_2 conversion in CXEs, results from COMSOL simulations of experimental electrocatalytic data suggested that the inner-sphere electron transfer rates were slowed as the concentration of CO_2 in the liquid phase increased.[17,20] These observations highlight that pressure-dependent changes in solution conductivity could be accompanied by pressure-dependent changes in the composition and behavior of the near-electrode microenvironment composed of the double layer and/or reaction-diffusion regions.[31]

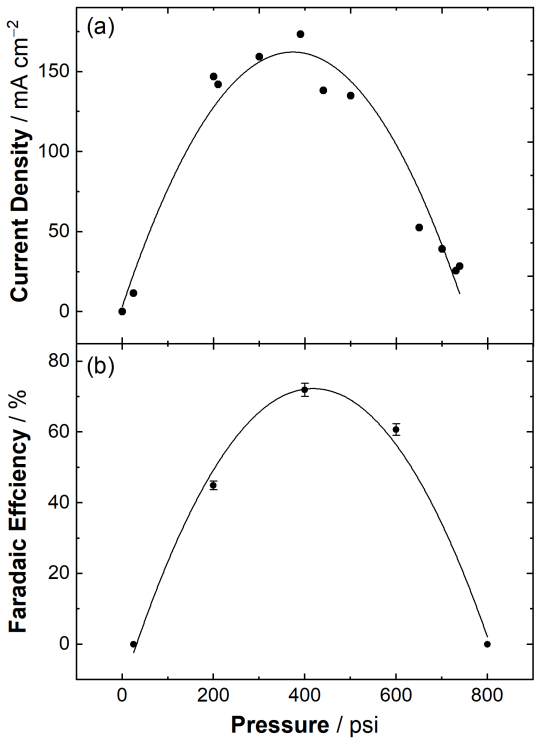

Figure 8. (a) Current density at −2.5 V *vs.* $Fc^{+/0}$ as a function of CO_2 pressure on polycrystalline Au as working electrode, counter electrode Pt wire, and reference electrode copper wire immersed in electrolyte solution and placed in a fritted chamber. This data was adapted for use in this paper from previous publication.[48] (b) Faradaic efficiency for electrocarboxylation of acetophenone to atrolactic acid as a function of pressure for 12 h bulk electrolysis experiments. Working electrode: glassy carbon, sacrificial counter electrode: magnesium rod, reference electrode: copper wire. Uncertainties (given as ±1σ) were calculated from replicate at 400 psi of CO_2. This data was adapted for use in this paper from a previous publication.[17]

Regarding this possibility, on the one hand the results of the electrochemical simulations reported here also show that the double layer capacitance[49] of the working electrode (1.0×10^{-5} F) was essentially invariant across the full range of CO_2 pressures explored in the work. In other words, there was no significant change in the non-Faradaic current flowing during cyclic voltammetry at each pressure. On the other hand, it is known that these currents depend on the structure and composition of the electrochemical double layer, and thus an interesting opportunity for future work would be to compare the bulk concentration of CO_2 with that achieved near electrode surfaces. Significant quantities of CO_2 could change or disrupt the structure of this important region, and comparisons of such near-surface, microenvironment effects could reveal the roles of surface chemistry and/or double-layer structure on CO_2 distribution in solution.

Dissolution of high concentrations of CO_2 provides an ample pool of substrate for electroconversion, but solution conductivity and electrolyte composition could also contribute to modulation of catalytic effectiveness, especially at the highest pressures in CXE-based systems. Such unexpected pressure-induced losses appear significant at the highest pressures, where even though there is a generous bulk supply of CO_2 available, resistive loss from charge transfer resistance could lead to increased effective overpotentials that diminish the energy storage efficiency in the carbon-based fuel or chemical being produced. In conventional electroanalytical work, data can be "corrected" for solution resistance changes through iR compensation[49] or are collected under low-

current conditions where resistive effects are minimized.[50] In practical electrosynthetic work, such ad-hoc modifications to reported data are not useful for meaningfully overcoming efficiency losses, in that total cell voltages will be higher in systems with diminished solution conductivities. Considering the results reported here, electrolyte engineering to optimize across the competing factors that influence electrocatalytic effectiveness appears to be critical for development of next-generation CO_2 conversion systems.

Moreover, in our work on electrosynthetic carboxylation of acetophenone to atrolactic acid on glassy carbon, electrokinetic data were not corrected by iR compensation, as low currents were involved in most experiments.[17] Similarly, in the molecular work with $Re(bpy)(CO)_3Cl$, kinetic data were analyzed by foot-of-the-wave analysis (FOWA)[50] at the recommended low-current region of catalytic waves. However, despite these factors that should compensate for the conductivity effects elucidated here in the identical CXEs used for these processes, there still appears to be significant loss of catalysis at around 450 psi of CO_2. Work utilizing a Au electrode underwent post-run iR correction of voltammetry data collected at 750 psi of CO_2, but this correction did not enable recapitulation of current to that measured at the lower, optimum pressure of 460 psi of CO_2.[19] The molecular dynamics simulations reported here highlight that greater concentrations of CO_2 significantly increase ion pairing in the electrolyte, and this change in behavior, along with others, could impact catalysis beyond 450 psi.

The loss of catalytic efficiency at the highest of pressures is secondary, however, to the overall enhancement seen in the achievable current densities (by more than two orders of magnitude in the case of electrocatalytic CO_2 reduction as shown in Figure 8a). Indeed, the best enhancement is achieved at pressures (~450 psi) that are well below the top of our CXE range of 800 psi. Inspection of the literature confirms that the pressure of the optimum in our studies is much lower than the pressures used in existing industrial chemical processes. For reference, industrial 1-octene hydroformylation is performed at approximately 3000 psi[51] while the decaffeination of coffee beans relies on supercritical CO_2 and requires pressures exceeding 1150 psi.[52] These comparisons point toward CXEs being realistically feasible media for development, as they require lower pressures than those used at large scales currently. And, if CXEs could be brought to practical implementation, the enhanced rates made possible with CXEs would favor scalability, in that smaller cell/reactor volumes would be required to meet productivity targets.

In terms of specific productivity targets, one could look to existing electrochemical technologies to contextualize CXE conductivities. For example, a common alkaline electrolyte used for H_2 generation by electrolysis is 2 M KOH; such a solution achieves a conductivity of 0.325 S cm^{-1}, a value that is an order of magnitude greater than that achieved here with CXEs.[53] However, it is important to note that such high concentrations of salt can drive precipitation of solids on cell cathodes, significantly limiting device performance despite the appealing high conductivity of the bulk solution.[21] And, such an alkaline solution likely could not be used for CO_2 electrolysis due to carbonate formation/precipitation. Thus, much like in CXEs, there are important tradeoffs to consider in optimal system design. Along this line, proton exchange membranes (PEMs) in PEM-based electrolyzers achieve even higher conductivities of ca. 5-65 S cm^{-1}, but appear to face significant stability limitations during prolonged operation that obviate the appealing nature of the high membrane/electrolyte conductivity.[54,55] Considering all these comparisons and technological trade-offs, we anticipate that understanding of the fundamental, molecular interactions that govern electrochemical behaviors in CO_2-containing electrolytes will ultimately enable progress toward efficient next-generation CO_2 electro-conversion schemes. In the case of CO_2 conversion chemistry, the most attractive approaches will no doubt harness the unique properties of CO_2, taking advantage of this molecule's uncommon profile of physico-chemical features to overcome challenges in its conversion to useful, "green" chemicals and fuels.

4. CONCLUSION

Molecular engineering of CO_2-rich electrolyte solutions is an underappreciated approach to improving the performance of electrochemical systems designed for CO_2 conversion. Here, we have used a joint experimental-theoretical approach to show that the conductivity of CO_2-rich electrolytes containing a liquid organic solvent and a suitable soluble salt, a class of media we have termed CXEs, display an unusual two-regime behavior of the pressure-dependent conductivity. MD simulations have been used to reveal the fundamental interactions between the solution components that drive this unusual behavior at a molecular level, including most importantly a compensation of decreased ionic strength and charge screening with increased ionic mobilities that enables stable solution conductivity up to 4 M CO_2. Taken together, these results shed light on the mechanisms underpinning electrolyte conductivity in the presence of CO_2 and reveal that dissolution of CO_2, although nonpolar by its very nature, can be leveraged to impart improved mass transport, a useful result that could impact design of next-generation systems for CO_2 conversion.

5. EXPERIMENTAL SECTION

5.1. General Considerations. All manipulations were carried out in dry N_2-filled glovebox (Vacuum Atmospheres Co., CA, USA) or under Ar atmosphere in a glovebag unless otherwise noted. All solvents were of commercial grad and dried over activated alumina by using a PPT Contour (Nashua, NH) solvent purification system prior to use, and were stored over molecular sieves. All chemicals used were from major suppliers and used after extensive drying.

5.2. Electrochemical Experiments. Electrochemical experiments were either carried out in a N_2-filled glovebox or in a 50 mL reactor (Parr Instrument Co.) equipped with a custom machined lid outfitted with gas-tight electrical leads as was as a temperature probe and pressure transducer (sensitivity ±7 psi)[19] in dry, degassed CH_3CN. The supporting electrolyte used was tetra(n-butylammonium) hexafluorophosphate ($[nBu_4N][PF_6]$; oakwood chemical Co.). Electrochemical measurements were done with a Gamry reference 3000 Potentiostat/Galvanostat and Gamry Reference 600+ Potentiostat/Galvanostat (Gamry Instruments, Warminster, PA, USA) using a standard three-electrode setup.

Cyclic voltammetry utilized ferrocene (Sigma-Aldrich; twice sublimed) and cell setup with basal plane of highly oriented pyrolytic graphite (HOPG, GraphiteStore.com, Buffalo Grobe, Ill.; A=0.15 cm^2) as working electrode, platinum wire (Kurt J. Lesker, Jefferson Hills, PA, USA; 99.99%, 0.5 mm diameter) for reference and counter electrodes. Concentration of ferrocene was kept constant at each selected pressure by adjusting initial concentration of ferrocene with VE curve to be 2 mM upon dilution from expansion with CO_2.

Electrochemical impedance spectroscopy for conductivity measurements was performed with custom designed Jones-geometry conductivity device previously discussed in section 2.3. Solution resistance values used for conductivity calculations were from the high frequency point of EIS.[56]

Electrochemical reactor studies proceed with electrolyte solutions loaded into the reactor under Ar atmosphere in a glovebag. Prior to experiments, the reactor was purged three times by repeated pressurization and depressurization cycles (~100 psi to ~30 psi) to exclude trace water and oxygen from the system. To achieve liquid expansion, the reactor was brought to the required pressure stirred only until equilibrium

was established, and then closed off from the gas supply and stirring turned off for experiments.

5.3. Electrochemical Simulations. Electrochemical digital simulations were conducted using the program DigiElch. Experimental cyclic voltammetry was uploaded to the software along with known parameters for double layer capacitance, resistance, electrode area, temperature, heterogenous electron transfer rate, and concentration of the electroactive species. Output from these simulations is diffusion coefficient and fitted cyclic voltammetry.

5.4. Conductivity Device. Conventionally, conductivity measurements must be carried out with parallel-facing macro-electrodes that have virtually identical cross-sectional areas and surface preparations. In this Jones-type geometry, the intrinsic solution conductivity can be measured in accord with NIST recommendations. Placement of two parallel Pt foil electrodes with a fixed separation within a glass tube is the typical layout used for such measurements.[34] Considering this, the resistance values collected through CVs (*vide supra*) are useful for observing some trends but cannot be used to rigorously quantify the intrinsic solution conductivity, as different materials were required for the working and reference electrodes and the geometry achievable in our pressure reactor with these electrodes cannot satisfy the design criterion of the Jones-type geometry. In particular, achievement of the Jones-type geometry was found to be critical and consequently we developed a capability to carry out such measurements in our reactor.

We were inspired in this effort by the basic designs of Jones-type cells that have been reported in prior work [34,57] The design that ultimately proved effective here is shown in Figure S3, and relies on the *de facto* standard electrode material, platinum, for fabrication of the two parallel flag electrodes. Pt wires were attached to the back of each flag electrode; the wires were subsequently encased in glass to prevent solution contact, giving a consistent geometric area defined solely by the platinum foil. Careful glassblowing enabled use of the resulting device under pressurized conditions. However, a fully sealed tube for separation of the electrodes and holding of the working solution was not utilized; instead, the electrodes are held a set distance apart by two solid glass support rods. In line with literature procedures, we were able to determine the cell constant of our device by calibration with a standard 1.0 M aqueous KCl solution of a known conductivity (0.113 S/cm)(Figure S4) held at 25°C.[58] With this method, we determined our cell constant to be 0.242 cm^{-1}.

5.5. Theory. From molecular dynamics simulations, generalized self-diffusion coefficients (D_α) and correlated diffusion coefficients ($D_{\alpha\gamma}$) were calculated from the corresponding mean-squared displacements (MSD_α and $MSD_{\alpha\gamma}$), where α and γ denote ion types and can represent either a cation or an anion. The self-MSD, *i.e.*, for cations or anions, is calculated as

$$MSD_\alpha(t) = \frac{1}{N_\alpha}\sum_i^{N_\alpha}[\vec{r}_i(t) - \vec{r}_i(0)]^2 \qquad (2)$$

where $\vec{r}_i(t)$ is the position vector of ion *i*'s central atom at time *t* and N_α is the total number of ions of type α. The correlated MSD between components α and γ, *i.e.*, cation-cation, anion-anion, or cation-anion, can be calculated as

$$MSD_{\alpha\gamma}(t) = \frac{(1+\delta_{\alpha\gamma})}{N_\alpha(N_\gamma-\delta_{\alpha\gamma})}\sum_i^{N_\alpha}\sum_{j'}^{N_\gamma}[\vec{r}_i(t) - \vec{r}_i(0)]\left[\vec{r}_j(t) - \vec{r}_j(0)\right]. \qquad (3)$$

where $\delta_{\alpha\gamma}$ is 1 when ion type $\alpha=\gamma$ and 0 when ion type $\alpha\neq\gamma$. Note that j' indicates the second sum is over $j \neq i$ when $\alpha=\gamma$. From MSD_α, the self-diffusion coefficient can be calculated as

$$D_\alpha = \lim_{t\to long}\frac{MSD_\alpha(t)}{6t}\ . \qquad (4)$$

The correlated diffusion coefficient $D_{\alpha\gamma}$ can similarly be calculated from $MSD_{\alpha\gamma}$.

The solution conductivity was calculated using the Einstein relation and has contributions from both the self-diffusion and correlated diffusion coefficients:

$$\sigma_\alpha = \frac{N_\alpha z_\alpha e^2}{V k_B T} D_\alpha, \qquad (5)$$

and

$$\sigma_{\alpha\gamma} = \frac{N_\alpha(N_\gamma-\delta_{\alpha\gamma})z_\alpha z_\gamma e^2}{V k_B T\,(1+\delta_{\alpha\gamma})} D_{\alpha\gamma}, \qquad (6)$$

where *e* is the elementary charge, *V* is the volume of the simulation box, k_B is Boltzmann's constant, *T* is temperature, and z_α and z_γ are the ionic charges of types α and γ, respectively.[59] The total solution conductivity can be represented as the sum of the contributions from the self-diffusion and correlated diffusion terms[60]

$$\sigma = \sigma_{cation} + \sigma_{anion} + \sigma_{cation-cation} + \sigma_{anion-anion} + 2\sigma_{cation-anion}\ . \qquad (7)$$

Note that since $\sigma_{\alpha\gamma} = \sigma_{\gamma\alpha}$, there is a coefficient of 2 in front of $\sigma_{cation-anion}$. The shear viscosity (η_s) was calculated using the Green-Kubo relation

$$\eta_s = \frac{V}{k_B T}\int_0^\infty \langle P_{ab}(0)P_{ab}(t)\rangle dt \qquad (8)$$

where P_{ab} is an average of the five autocorrelation functions from the anisotropic terms of the stress tensor: P_{xy}, P_{yz}, P_{xz}, (P_{xx}-P_{yy})/2, and (P_{yy}-P_{zz})/2.[61]

The coordination number was calculated from the radial pair distribution function (RDF) [61]

$$g(r) = \frac{V}{N^2}\left\langle\sum_i\sum_{j\neq i}\delta\left(r - \left|\vec{r}_{ij}\right|\right)\right\rangle \qquad (9)$$

Where N is the number of molecules and $\vec{r}_{ij} = \vec{r}_i - \vec{r}_j$. From the RDF, coordination numbers can be calculated as

$$n(r') = \rho\int_0^{r'} 4\pi r^2 g(r)dr \qquad (10)$$

Where ρ is the number density and $4\pi r^2$ is the volume of the solvation shell with cutoff distance r', which is taken to be the location of the first minimum in the RDF, 7.35-7.44 Å depending on CO_2 pressure.

ASSOCIATED CONTENT

The Supporting Information is available free of chart at https://pubs.acs.org/doi/10.1021/###
Supplementary details on the theoretical methods; electrochemical data; results from electrochemical simulations; electrochemical impedance spectroscopy measurements (PDF)

ACKNOWLEDGMENT

The authors thank Jim Hodgson (Kansas State University) and Dan Hastert (University of Kansas) for assistance with fabrication of the Jones-geometry conductivity device. This work was supported by the US National Science Foundation through awards CBET-1605524 and CHE-2102656. C.K.N. and M.A.S. were supported by a U.S. National Science Foundation Research Traineeship (NRT) at the University of

Kansas (DGE-1922649). This material is also based upon work by E.R.B. that was supported by the Madison & Lila Self Graduate Fellowship at the University of Kansas.

Corresponding Author E-mail Addresses

James D. Blakemore: blakemore@ku.edu
Ward H. Thompson: wthompson@ku.edu
Bala Subramaniam: bsubramaniam@ku.edu
Kevin C. Leonard: kcleonard@ku.edu

REFERENCES

[1] Gao, D.; Arán-Ais, R. M.; Jeon, H. S.; Roldan Cuenya, B., Rational catalyst and electrolyte design for CO_2 electroreduction towards multicarbon products. *Nat. Catal.* **2019,** *2*, 198-210.

[2] Yang, J.; Kang, X.; Jiao, J.; Xing, X.; Yin, Y.; Jia, S.; Chu, M.; Han, S.; Xia, W.; Wu, H.; He, M.; Han, B., Ternary Ionic-Liquid-Based Electrolyte Enables Efficient Electro-reduction of CO_2 over Bulk Metal Electrodes. *J. Am. Chem. Soc.* **2023,** *145*, 11512-11517.

[3] Vichou, E.; Solé-Daura, A.; Mellot-Draznieks, C.; Li, Y.; Gomez-Mingot, M.; Fontecave, M.; Sánchez-Sánchez, C. M., Electrocatalytic Conversion of CO_2 to Formate at Low Overpotential by Electrolyte Engineering in Model Molecular Catalysis. *ChemSusChem* **2022,** *15*, e202201566.

[4] Zhao, T.; Li, J.; Liu, J.; Liu, F.; Xu, K.; Yu, M.; Xu, W.; Cheng, F., Tailoring the Catalytic Microenvironment of Cu_2O with SiO_2 to Enhance C^{2+} Product Selectivity in CO_2 Electroreduction. *ACS Catal.* **2023,** *13*, 4444-4453.

[5] Resasco, J.; Chen, L. D.; Clark, E.; Tsai, C.; Hahn, C.; Jaramillo, T. F.; Chan, K.; Bell, A. T., Promoter Effects of Alkali Metal Cations on the Electrochemical Reduction of Carbon Dioxide. *J. Am. Chem. Soc.* **2017,** *139*, 11277-11287.

[6] Yuan, G.-Q.; Jiang, H.-F.; Lin, C.; Liao, S.-J., Efficient electrochemical synthesis of 2-arylsuccinic acids from CO_2 and aryl-substituted alkenes with nickel as the cathode. *Electrochim. Acta* **2008,** *53*, 2170-2176.

[7] Lv, J.-J.; Yin, R.; Zhou, L.; Li, J.; Kikas, R.; Xu, T.; Wang, Z.-J.; Jin, H.; Wang, X.; Wang, S., Microenvironment Engineering for the Electrocatalytic CO_2 Reduction Reaction. *Angew Chem. Int. Ed.* **2022,** *61*, e202207252.

[8] Dolmanan, S. B.; Böhme, A.; Fan, Z.; King, A. J.; Fenwick, A. Q.; Handoko, A. D.; Leow, W. R.; Weber, A. Z.; Ma, X.; Khoo, E.; Atwater, H. A.; Lum, Y., Local microenvironment tuning induces switching between electrochemical CO_2 reduction pathways. *J. Mater. Chem. A* **2023,** *11*, 13493-13501.

[9] Lv, J.-J.; Yin, R.; Zhou, L.; Li, J.; Kikas, R.; Xu, T.; Wang, Z.-J.; Jin, H.; Wang, X.; Wang, S., Microenvironment Engineering for the Electrocatalytic CO_2 Reduction Reaction. *Angew. Chem. Int. Ed.* **2022,** *61*, e202207252.

[10] Wu, H.; Singh-Morgan, A.; Qi, K.; Zeng, Z.; Mougel, V.; Voiry, D., Electrocatalyst Microenvironment Engineering for Enhanced Product Selectivity in Carbon Dioxide and Nitrogen Reduction Reactions. *ACS Catal.* **2023,** *13*, 5375-5396.

[11] Singh, M. R.; Kwon, Y.; Lum, Y.; Ager, J. W., III; Bell, A. T., Hydrolysis of Electrolyte Cations Enhances the Electrochemical Reduction of CO_2 over Ag and Cu. *J. Am. Chem. Soc.* **2016,** *138*, 13006-13012.

[12] Gao, D.; McCrum, I. T.; Deo, S.; Choi, Y.-W.; Scholten, F.; Wan, W.; Chen, J. G.; Janik, M. J.; Roldan Cuenya, B., Activity and Selectivity Control in CO_2 Electroreduction to Multicarbon Products over CuOx Catalysts via Electrolyte Design. *ACS Catal.* **2018,** *8*, 10012-10020.

[13] Murata, A.; Hori, Y., Product Selectivity Affected by Cationic Species in Electrochemical Reduction of CO_2 and CO at a Cu Electrode. *Bull. Chem. Soc. Jpn* **1991,** *64*, 123-127.

[14] Ren, S.; Joulié, D.; Salvatore, D.; Torbensen, K.; Wang, M.; Robert, M.; Berlinguette, C. P., Molecular electrocatalysts can mediate fast, selective CO_2 reduction in a flow cell. *Science* **2019,** *365*, 367-369.

[15] Yang, K.; Kas, R.; Smith, W. A.; Burdyny, T., Role of the Carbon-Based Gas Diffusion Layer on Flooding in a Gas Diffusion Electrode Cell for Electrochemical CO_2 Reduction. *ACS Energy Lett.* **2021,** *6*, 33-40.

[16] Möller, T.; Ngo Thanh, T.; Wang, X.; Ju, W.; Jovanov, Z.; Strasser, P., The product selectivity zones in gas diffusion electrodes during the electrocatalytic reduction of CO_2. *Energy Environ. Sci.* **2021,** *14*, 5995-6006.

[17] Stalcup, M. A.; Nilles, C. K.; Lee, H.-J.; Subramaniam, B.; Blakemore, J. D.; Leonard, K. C., Organic Electrosynthesis in CO_2-eXpanded Electrolytes: Enabling Selective Acetophenone Carboxylation to Atrolatic Acid. *ACS Sustainable Chem. Eng.* **2021,** *9*, 10431-10436.

[18] Sconyers, D. J.; Shaughnessy, C. I.; Lee, H.-J.; Subramaniam, B.; Leonard, K. C.; Blakemore, J. D., Molecular Electrocatalysis of CO2 Reduction with Pressure-Tunable CO_2-Expanded Electrolytes. *ChemSusChem* **2020,** *13*, 6338-6345.

[19] Shaughnessy, C. I.; Sconyers, D. J.; Kerr, T. A.; Lee, H.-J.; Subramaniam, B.; Leonard, K. C.; Blakemore, J. D., Intensified Electrocatalytic CO_2 Conversion in Pressure-Tunable CO_2-Expanded Electrolytes. *ChemSusChem* **2019,** *12*, 3761-3768.

[20] Shaughnessy, C. I.; Sconyers, D. J.; Lee, H. J.; Subramaniam, B.; Blakemore, J. D.; Leonard, K. C., Insights into pressure tunable reaction rates for electrochemical reduction of CO_2 in organic electrolytes. *Green Chem.* **2020,** *22*, 2434-2442.

[21] Marcandalli, G.; Monteiro, M. C. O.; Goyal, A.; Koper, M. T. M., Electrolyte Effects on CO_2 Electrochemical Reduction to CO. *Acc. Chem. Res.* **2022,** *55*, 1900-1911.

[22] Doherty, M. D.; Grills, D. C.; Fujita, E., Synthesis of Fluorinated $ReCl(4,4'\text{-}R_2\text{-}2,2'\text{-bipyridine})(CO)_3$ Complexes and Their Photophysical Characterization in CH_3CN and Supercritical CO_2. *Inorg. Chem.* **2009,** *48*, 1796-1798.

[23] Roškar, V.; Dombro, R. A.; Prentice, G. A.; Westgate, C. R.; McHugh, M. A., Comparison of the dielectric behavior of mixtures of methanol with carbon dioxide and ethane in the mixture-critical and liquid regions. *Fluid Phase Equilib.* **1992,** *77*, 241-259.

[24] Zeigermann, P.; Valiullin, R., Transport properties of gas-expanded liquids in bulk and under confinement. *J. Supercrit. Fluids* **2013,** *75*, 43-47.

[25] Rahmanian, A.; Ghaziaskar, H. S., Selective extraction of maleic acid and phthalic acid by supercritical carbon dioxide saturated with trioctylamine. *J. Supercrit. Fluids* **2008,** *46*, 118-122.

[26] Jessop, P. G.; Subramaniam, B., Gas-Expanded Liquids. *Chem. Rev.* **2007,** *107*, 2666-2694.

[27] Wei, M.; Musie, G. T.; Busch, D. H.; Subramaniam, B., CO_2-Expanded Solvents: Unique and Versatile Media for Performing Homogeneous Catalytic Oxidations. *J. Am. Chem. Soc.* **2002,** *124*, 2513-2517.

[28] Kordikowski, A.; Schenk, A. P.; Van Nielen, R. M.; Peters, C. J., Volume expansions and vapor-liquid equilibria of binary mixtures of a variety of polar solvents and certain near-critical solvents. *J. Supercrit. Fluids* **1995,** *8*, 205-216.

[29] Scurto, A. M.; Hutchenson, K.; Subramaniam, B., Gas-Expanded Liquids: Fundamentals and Applications. In *Gas-Expanded Liquids and Near-Critical Media*, American Chemical Society: 2009; Vol. 1006, pp 3-37.

[30] Astruc, D., Why is Ferrocene so Exceptional? *Eur. J. Inorg. Chem.* **2017,** *2017*, 6-29.

[31] Savéant, J.-M.; Costentin, C., *Elements of Molecular and Biomolecular Electrochemistry*. Second Edition ed.; Wiley: 2019; pp. 6-15.

[32] Hopkins Leseberg, J. A.; Lionetti, D.; Day, V. W.; Blakemore, J. D., Electrochemical Kinetic Study of [Cp*Rh] Complexes Supported by Bis(2-pyridyl)methane Ligands. *Organometallics* **2021,** *40*, 266-277.

[33] Scurto, A. M.; Hutchenson, K.; Subramaniam, B., Gas-Expanded Liquids: Fundamentals and Applications. In *Gas-Expanded Liquids and Near-Critical Media*, American Chemical Society: 2009; Vol. 1006, pp 3-37.

[34] R. H. Shreiner, K. W. P., *Standard Reference materials: Primary Standards and Standard Reference Materials for Electrolytic Conductivity*. U.S. Government Printing Office: 2004; p 26.

[35] Morin Caamano, T.; Houache, M. S. E.; Sandoval, M. G.; Couillard, M.; Weck, A.; Baranova, E. A.; Abu-Lebdeh, Y., Tuning the Polarity of Dinitrile-Based Electrolyte Solutions for CO_2 Electroreduction on Copper Catalysts. *J. Phys. Chem. C* **2023,** *127*, 7230-7238.

[36] LeSuer, R. J.; Buttolph, C.; Geiger, W. E., Comparison of the Conductivity Properties of the Tetrabutylammonium Salt of Tetrakis(pentafluorophenyl)borate Anion with Those of Traditional Supporting Electrolyte Anions in Nonaqueous Solvents. *Anal. Chem.* **2004,** *76*, 6395-6401.

[37] (a) John R. Rumble, ed., CRC Handbook of Chemistry and Physics, 104th Edition (Internet Version 2023), CRC Press/Taylor & Francis, Boca Raton, FL; p. 6-231. (b) John R. Rumble, ed., CRC Handbook of Chemistry and Physics, 104th Edition (Internet Version 2023), CRC Press/Taylor & Francis, Boca Raton, FL; p. 6-233. (c) John R. Rumble, ed., CRC Handbook of Chemistry and Physics, 104th Edition (Internet Version 2023), CRC Press/Taylor & Francis, Boca Raton, FL; p. 8-30.

[38] Plimpton, S., Fast Parallel Algorithms for Short-Range Molecular Dynamics. *J. Comput. Phys.* **1995,** *117*, 1-19.

[39] Shoemaker, D. P.; Garland, C. W.; Steinfeld, J. I. *Experiments in physical chemistry*; McGraw-Hill, 2018; pp 47-49.

[40] A. Nitzan, *Chemical Dynamics in Condensed Phases. Relaxation, Transfer, and Reactions in Condensed Molecular Systems* (Oxford University Press, New York, 2006); pp. 414-415.

[41] Kubo, R. Statistical Mechanical Theory of Irreversible Processes. I. General Theory and Simple Applications to Magnetic and Conduction Problems. *J. Phys. Soc. Japan* **12,** 570–586 (1957).

[42] Marcandalli, G.; Goyal, A.; Koper, M. T. M., Electrolyte Effects on the Faradaic Efficiency of CO_2 Reduction to CO on a Gold Electrode. *ACS Catal.* **2021,** *11*, 4936-4945.

[43] Xu, K., Nonaqueous Liquid Electrolytes for Lithium-Based Rechargeable Batteries. *Chem. Rev.* **2004,** *104*, 4303-4418.

[44] Blanco, D. E.; Atwi, R.; Sethuraman, S.; Lasri, A.; Morales, J.; Rajput, N. N.; Modestino, M. A., Effect of Electrolyte Cations on Organic Electrosynthesis: The Case of Adiponitrile Electrochemical Production. *J. Electrochem. Soc.* **2020,** *167*, 155526.

[45] Ue, M.; Ida, K.; Mori, S., Electrochemical Properties of Organic Liquid Electrolytes Based on Quaternary Onium Salts for Electrical Double-Layer Capacitors. *J. Electrochem. Soc.* **1994,** *141*, 2989.

[46] Chen, Y.; Lewis, N. S.; Xiang, C., Operational constraints and strategies for systems to effect the sustainable, solar-driven reduction of atmospheric CO_2. *Energy Environ. Sci.* **2015,** *8*, 3663-3674.

[47] García de Arquer, F. P.; Dinh, C.-T.; Ozden, A.; Wicks, J.; McCallum, C.; Kirmani, A. R.; Nam, D.-H.; Gabardo, C.; Seifitokaldani, A.; Wang, X.; Li, Y. C.; Li, F.; Edwards, J.; Richter, L. J.; Thorpe, S. J.; Sinton, D.; Sargent, E. H., CO_2 electrolysis to multicarbon products at activities greater than 1 A cm^{-2}. *Science* **2020,** *367*, 661-666.

[48] Shaughnessy, C. I.; Sconyers, D. J.; Kerr, T. A.; Lee, H.-J.; Subramaniam, B.; Leonard, K. C.; Blakemore, J. D., Intensified Electrocatalytic CO_2 Conversion in Pressure-Tunable CO_2-Expanded Electrolytes. *ChemSusChem* **2019,** *12*, 3761-3768.

[49] Bard, A. J.; Faulkner, L., *Electrochemical Methods: Fundamentals and Applications*. Second edition ed.; Wiley: 2000; p. 9.

[50] Costentin, C.; Drouet, S.; Robert, M.; Savéant, J.-M. Turnover Numbers, Turnover Frequencies, and Overpotential in Molecular Catalysis of Electrochemical Reactions. Cyclic Voltammetry and Preparative-Scale Electrolysis. *J. Am. Chem. Soc.* **2012**, *134*, 11235-11242.

[51] E. Billig and D. R. Bryan, Oxo Process. In *Kirk-Othmer Concise Encyclopedia of Chemical Technology*, (Hoboken, NJ: Wiley-Interscience, 2000); p. 3.

[52] Katz, S. N. Working Knowledge Decaffeinating Coffee. In *Scientific American*, 1997; p. 148.

[53] Cofell, E. R.; Nwabara, U. O.; Bhargava, S. S.; Henckel, D. E.; Kenis, P. J. A. Investigation of Electrolyte-Dependent Carbonate Formation on Gas Diffusion Electrodes for CO_2 Electrolysis. *ACS Applied Materials & Interfaces* **2021**, *13*, 15132-15142.

[54] Mazúr, P.; Polonský, J.; Paidar, M.; Bouzek, K. Non-conductive TiO_2 as the anode catalyst support for PEM water electrolysis. *Int. J. Hydrogen Energy* **2012**, *37*, 12081-12088.

[55] Puthiyapura, V. K.; Mamlouk, M.; Pasupathi, S.; Pollet, B. G.; Scott, K. Physical and electrochemical evaluation of ATO supported IrO_2 catalyst for proton exchange membrane water electrolyser. *J. Power Sources* **2014**, *269*, 451-460.

[56] Orazem, M. E., *Electrochemical Impedance Spectrocopy*. Second edition ed.; Wiley: Hoboken, New Jersey, 2017; p. 471.

[57] Wu, Y. C.; Koch, W. F., Absolute determination of electrolytic conductivity for primary standard KCl solutions from 0 to 50°C. *J. Solution Chem.* **1991,** *20*, 391-401.

[58] Mozhzhukhina, N.; Longinotti, M. P.; Corti, H. R.; Calvo, E. J., A conductivity study of preferential solvation of lithium ion in acetonitrile-dimethyl sulfoxide mixtures. *Electrochim. Acta* **2015,** *154*, 456-461.

[59] Kubisiak, P.; Wróbel, P.; Eilmes, A., Molecular Dynamics Investigation of Correlations in Ion Transport in MeTFSI/EMIM–TFSI (Me = Li, Na) Electrolytes. *J. Phys. Chem. B* **2020,** *124*, 413-421.

[60] Gullbrekken, Ø.; Røe, I. T.; Selbach, S. M.; Schnell, S. K., Charge Transport in Water–NaCl Electrolytes with Molecular Dynamics Simulations. *J. Phys. Chem. B* **2023,** *127*, 2729-2738.

[61] Allen, M. P.; Tildesley, D. J. *Computer Simulation of Liquids*; Oxford University Press, 2017; p. 60.

TOC Graphic:

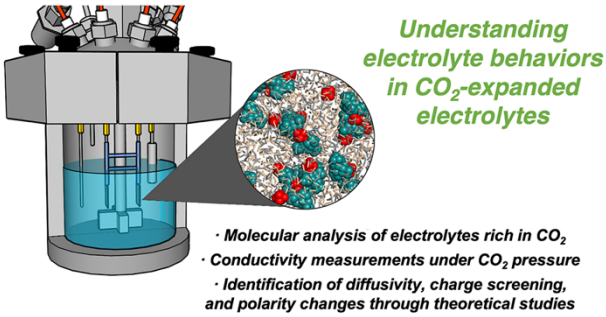

TOC Synopsis: The molecular design of electrolytes for use in electrochemical systems for CO_2 conversion is an important topic, but the effect of dissolution of large concentrations of CO_2 on bulk solution properties has received less attention than it deserves. Here, the effect of CO_2 dissolution on solution conductivity has been quantified, revealing that dissolution of nonpolar CO_2 can promote solution conductivity through increasing the diffusivity of cations and anions in solution. Molecular dynamics simulations also reveal the fundamental interactions that drive diminished conductivity at higher concentrations of CO_2, providing a comprehensive view of the mechanisms underpinning electrolyte behaviors in electrochemical systems containing CO_2.